

# Collisionless dynamics in Globular Clusters

Liliya L. R. Williams,<sup>1\*</sup> Eric I. Barnes,<sup>2†</sup> Jens Hjorth,<sup>3‡</sup>

<sup>1</sup>*School of Physics and Astronomy, University of Minnesota, 116 Church Street SE, Minneapolis, MN 55455, USA*

<sup>2</sup>*Department of Physics, University of Wisconsin — La Crosse, La Crosse, WI 54601, USA*

<sup>3</sup>*Dark Cosmology Centre, Niels Bohr Institute, University of Copenhagen, Juliane Maries Vej 30, DK-2100 Copenhagen Ø, Denmark*

13 November 2018

## ABSTRACT

Since globular clusters (GCs) are old, low- $N$  systems their dynamics is widely believed to be fully dominated by collisional two-body processes, and their surface brightness profiles are fit by King models. However, for many GCs, especially those with HST-resolved central regions, and ‘extra-tidal’ features, King models provide poor fits. We suggest that this is partly because collisionless dynamics is also important and contribute to shaping the cluster properties. We show using time-scale and length-scale arguments that except for the very centers of clusters, collisionless dynamics should be more important than collisional. We then fit 38 GCs analyzed by Noyola & Gebhardt (2006) with (collisional) King and (collisionless) DARKexp models over the full available radial range, and find that the latter provide a better fit to 29 GCs; for six of these the fit is at least  $\sim 5\times$  better in term of *rms*. DARKexp models are theoretically derived maximum entropy equilibrium states of self-gravitating collisionless systems and have already been shown to fit the results of dark matter N-body simulations. (We do not attempt fits with ad hoc fitting functions.)

**Key words:**

## 1 INTRODUCTION

Globular Clusters (GCs) are old and contain a relatively small number ( $\sim 10^5 - 10^6$ ) of stars, as compared to galaxies, and are therefore believed to have relaxed through two-body encounters, both strong and weak. In a Hubble time some GCs would have formed many compact binaries, reached core collapse, and possibly undergone several gravothermal oscillations (Elson et al. 1987; Meylan & Heggie 1997).

The theoretical treatment of this gravitational evolution problem is not straightforward. While it is possible to describe realistic thermal equilibria for self-gravitating systems (see § 3), the negative heat capacity of such systems implies that these equilibria are not stable. Any reduction in total energy leads to an increase in the kinetic temperature of the system, however, it is reasonable to assume that if GCs evolve slowly enough they go from one quasi-equilibrium state to another. These quasi-equilibrium states are often described by King equilibrium models, which attempt to take into account two key characteristics of GCs: relaxation through two-body encounters, and Galactic tidal field. To incorporate these characteristics, King (1966) starts with the Maxwell-Boltzmann distribution function,

$f(E) \propto \exp([\Phi_0 - E]/\sigma^2)$ , which corresponds to the isothermal sphere of central potential  $\Phi_0$  and constant velocity dispersion  $\sigma$ , and truncates it to imitate the result of spatial tidal stripping experienced by systems in the Galactic tidal field,  $f(E) \propto \exp([\Phi_0 - E]/\sigma^2) - 1$ ; see also Michie (1963). King-Michie models extend isotropic King models to include velocity dispersion anisotropy.

It is generally believed that GCs are well-fit by King, or King-Michie models (Elson et al. 1987; Meylan & Heggie 1997). However, deviations from King models have always been known to exist, both at small and large radii. At small radii, the central density profiles, especially in HST data, sometimes lack the flat density cores required by King models but instead exhibit a range of power-law cusps (Noyola & Gebhardt 2006). At large radii, many clusters are better fit with power-law density profiles that remain shallower than King to the last observable point (McLaughlin & van der Marel 2005; Carballo-Bello et al. 2012). Other GCs appear to contain ‘extra-tidal’ stars, which make the surface brightness profiles more extended than King models.

Because some GCs are known to show mass segregation, many authors argue that GCs should be fit with multiple King models, each representing some narrow stellar mass range. Profiles consisting of several (and as many as 10) mass components have been presented (Da Costa & Freeman 1976). Several authors have also pointed out that models other than King can provide more conforming fits, like

\* email: llrw@astro.umn.edu

† email: barnes.eric@uwlax.edu

‡ email: jens@dark-cosmology.dk

Wilson models (Wilson 1975; McLaughlin & van der Marel 2005), or the power law models (Carballo-Bello et al. 2012). The main drawback of using the latter two models is that they are ad hoc fitting functions.

We are motivated by the widespread deviations between observations and King models and the wide variety of proposed fixes to ask whether King is really the best basic model for GCs. More specifically, we ask if the two-body encounters that involve one or few stars are as dominant a feature as it is generally believed, or if collective collisionless effects on scales of hundreds or thousands of stars are also important.

There is a possible indication of collisionless dynamics in at least one cluster. WLM-1, studied in detail by Stephens et al. (2006), has an ellipticity of  $e = 0.17$  which they conclude is not the result of rotation or Galactic tides. Instead, the shape is most likely due to anisotropic velocity dispersions, as occurs in many ellipticals. Two-body effects would have wiped out differences in velocity dispersion in different directions, which implies that two-body relaxation has not been very efficient in this GC.

Violent relaxation, a collisionless process, is brought about by fluctuations in the large-scale, or global potential of the system. The difference from collisional relaxation is that particles—stars—exchange energy with the large-scale potential, and not directly among themselves. In the case of galaxies, the potential fluctuations are usually the consequence of collapse and subsequent oscillations that occur during formation. In the case of GCs, the time since initial collapse is generally longer than the two-body relaxation time-scale, and so additional causes for global potential fluctuations might be necessary if collisionless relaxation is to be relevant for present-day GCs, such as GC's elliptical orbits in the Galaxy, disk passage, Galactic tides, and core collapse and bounce. For example, from the proper motion measurements of NCG 6397 Kalirai et al. (2007) conclude that the cluster has made frequent passages through the Galactic disk.

Mixing is another aspect of collisionless relaxation; it does not result in energy changes of particles, but is also thought to be important in the formation of galaxies (Merritt 2005). It is difficult to assign a specific mechanism responsibility, because even though the importance of potential fluctuations and mixing as drivers of collisionless relaxation is well established, the full understanding of relaxation and its detailed mechanics is still lacking. So instead of investigating the relaxation mechanisms, we take a different approach. As we describe in Section 3.2, it is possible to derive the final state attained by the system after collisionless relaxation is complete, with no regard for the dynamics that lead to it. The final relaxed state can be described by the mass density distribution, which can then be compared to that of GCs.

Therefore, in the present paper we do not undertake any dynamical experiments. We fit GC surface brightness (SB) profiles from the literature, with two functions: King and DARKexp, which represent fully collisional and fully collisionless systems, respectively. Section 3 shows that each model has been derived from maximum entropy arguments implying that these are effective quasi-equilibrium models for the final state of the two types of systems. We do not fit ad hoc or loosely motivated functions.

## 2 ASSESSING COLLISIONALITY OF GLOBULAR CLUSTERS

It is well established that two-body, or collisional processes are responsible for many properties of GCs, like the presence and hardening of binaries, mass segregation, and possibly energy transport and core collapse (Meylan & Heggie 1997).

Here we ask, how important are collisionless effects in Globular Clusters? One way to address the question is to estimate relevant time-scales. The two-body relaxation time-scale for GCs is shorter than the Hubble time. However, one must also compare it to the collisionless relaxation time-scale which proceeds on dynamical, or approximately crossing time-scales (Binney & Tremaine 1987; Lynden-Bell 1967).

The two-body relaxation time-scale is of the order,  $t_{2bd} = (r/v)N/(8 \ln N)$ , where  $r$  is the size of the system,  $v$  is the characteristic velocity of the particles, and  $N$  is the number of particles. The dynamical time-scale is,  $t_{dyn} = 2\pi(r/v_c)$ , where  $v_c$  is the circular velocity and is of the same order as  $v$ . The ratio of the two,  $t_{dyn}/t_{2bd} = 16\pi(\ln N)/N$  is 2.3 for  $N = 100$  and  $6 \times 10^{-3}$  for  $N = 10^5$ . This difference suggests that collisionless relaxation will drive the overall dynamical evolution of a GC, but interior to radii where  $N \sim 100$ , the two-body processes become more important for the evolution.

Another way to access the relevance of collisionless effects as a function of distance  $r$  from cluster center is to ask whether the cluster's acceleration field is grainy or smooth on the scale of individual stars. For this, one needs to estimate two length-scales. The first,  $r_{eq}$  is the distance from the star where the typical acceleration induced by that star equals the acceleration due to the global potential;

$$\frac{GM(< r)}{r^2} = \frac{Gm}{r_{eq}^2}. \quad (1)$$

Here, the total mass of the cluster is related to the mass of a single star, and the total number of stars,  $M_{tot} = mN_{tot}$ . The other length-scale,  $r_{sep}$ , is the typical separation between stars at radius  $r$ ,  $r_{sep} = [(4\pi/3)\rho(r)/m]^{-1/3}$ . The ratio of the two is

$$\frac{r_{sep}}{r_{eq}} = \left(\frac{3M_{tot}}{4\pi\rho(r)r^3}\right)^{1/3} \left(\frac{M(< r)}{M_{tot}}\right)^{1/2} N_{tot}^{1/6} \quad (2)$$

If  $r_{sep} \ll r_{eq}$ , as one would find near the center of a GC, then the acceleration field and the potential are grainy, so the situation is collisional.

Note that because this calculation assesses the graininess of the acceleration field (at distance  $r$ ), it includes all types of collisional encounters—the strong ones with nearby stars and the weak ones with more distant stars.

If  $r_{sep} \gg r_{eq}$ , for example, in the outer regions of a GC, then the acceleration field and the potential are smooth, and the situation is collisionless.

It is interesting to see how the two collisionality criteria, one based on time-scales and the other based on length-scales compare. In Figure 1 the top panels show the results of the time-scale argument, and the bottom panel, the length-scale argument. The top panel plots the fraction of the enclosed mass, or the fraction of the total number of particles as a function of radius. The horizontal axis is in units of  $r_{-2}$ , the radius at which the logarithmic space density slope  $\gamma = -d \log(\rho)/d \log(r)$ , is equal to 2. Above, it was deter-

mined that central regions where  $N < 100$  will be largely collisional. The horizontal dashed lines indicate this level for representative  $N_{tot}$  values of  $10^3$  and  $10^6$ . The bottom panel plots  $r_{sep}/r_{eq}$  vs. radius. Using the length-scale argument above, it was determined that  $r_{sep} \approx r_{eq}$  divides collisional from collisionless regimes. In the bottom panel, that division is represented by the dashed horizontal line at  $r_{sep} = 3r_{eq}$ . This specific relationship between  $r_{sep}$  and  $r_{eq}$  guarantees agreement between the time-scale and length-scale viewpoints for  $N_{tot} = 10^3$  and  $10^6$  systems, and for DARKexp and King density profiles. The vertical dashed lines highlight that in both the top and bottom panels the collisional/collisionless transition occurs at the same location in the system, for a given size and model.

We note that instead of  $t_{2bd}$  as an estimate of the two-body relaxation time-scale one could have chosen the Spitzer mean time-scale (Spitzer 1987) which is based on the diffusion rate of particles through phase-space due to encounters,

$$t_{sp} = 0.34 \frac{\sigma^3}{G^2 m \rho \ln \Lambda}. \quad (3)$$

Here,  $\sigma$ ,  $m$ ,  $\rho$  and  $\ln \Lambda$  are the velocity dispersion, average stellar mass, mass density, and the Coulomb logarithm, respectively. For the DARKexp and King density profiles of a range of shape parameters,  $t_{sp}$  is larger than  $t_{2bd}$  by at least a factor of 10 over the relevant radial ranges. Using the Spitzer time-scale would not have produced an agreement between time- and length-scales that we have in Figure 1, but since  $t_{sp}$  is always longer than  $t_{2bd}$  it makes two-body effects even less important than we have estimated.

We conclude that both time- and length-scale considerations lead to the same assessment of the collisionality of a system or part thereof, if  $t_{2bd}$  is used. And, regardless of how two-body relaxation is quantified, both approaches suggest that in a typical cluster with  $N_{tot} > 10^4$ , most of the body of the cluster, with the possible exception of the very center, would evolve collisionlessly.

### 3 MODELS

#### 3.1 King-Madsen models

Even though King models are physically motivated and have a full dynamical description provided by the King distribution function (DF), there did not exist a rigorous derivation of that DF until Madsen (1996). Madsen, like King and others before him, assumes that repeated two-body encounters in GCs require that one start with the Maxwellian velocity distribution and hence Maxwell-Boltzmann statistics which deal with classical particles that do not obey the exclusion principle.

Madsen finds that the equilibrium state can be obtained as the maximum entropy state. Unlike the standard derivation, which assumes that the occupation numbers in all energy states are always large and hence Stirling approximation is valid, he argues that no approximation should be made. Following Simons (1994), the exact form of the resulting DF is derived,  $f(E) = [Ag \exp(-\beta E)]$ , where  $[\cdot]$  means round down to the nearest integer, and  $A$ ,  $g$  are constants, and  $\beta$  is the constant inverse temperature of the system. This DF has discrete ‘steps’ that are especially pronounced at low occupation numbers. Its smooth version (Hjorth &

Williams 2010; Barnes & Williams 2012) is indistinguishable from the King DF. Madsen (1996) shows that when combined with the Poisson equation, his DF gives density profiles that are very similar to King’s, and Hjorth & Williams (2010); Barnes & Williams (2012) show that the smooth version of Madsen DF results in density profiles that are virtually identical to the standard King (1966) profiles.

Note that in the case of the King DF, ‘ $-1$ ’ was added by hand to imitate the action of the tidal field. In Madsen’s derivation, the corresponding modification of the DF results from a proper treatment of low occupation numbers.

#### 3.2 DARKexp models

It has long been realized that the smooth appearance of elliptical galaxies, which consist of tens of billions of stars, cannot be due to two-body relaxation processes, like the rare strong encounters between stars, or the numerous weak encounters. Some faster acting relaxation mechanism had to be at work to ensure that the bulk of the ellipticals relax in well under a Hubble time. This mechanism would involve a rapidly changing potential of the system, which would induce individual stars to change energy. Because the mechanism has to act fast, it was called ‘violent’ relaxation by Lynden-Bell (1967). It is an example of collisionless relaxation, because particles exchange energy with the global potential and not through strong or weak ‘collisions’ among themselves.

If we care only about the final state of the system and not the full dynamical history, we can use the tools of statistical mechanics. This approach to collisionless self-gravitating systems was originally put forward by Ogorodnikov (1957), and Lynden-Bell (1967), who argued that the final steady-state would correspond to the most likely state. Lynden-Bell (1967) incorporated the collisionless nature of the stellar flow through an exclusion principle in phase-space: the collisionless Boltzmann equation states that a collisionless fluid is incompressible, hence phase-space elements cannot be superimposed. In the non-degenerate limit, Lynden-Bell’s theory predicted that the maximum entropy states would be isothermal spheres, as was also found by Ogorodnikov (1957). However, this result is unsatisfactory. While the maximization procedure imposed constraints of finite mass and energy, isothermal spheres are infinite. Furthermore, elliptical galaxies look nothing like isothermal spheres. Several ways out of this problem were proposed in the following decades. (See the Hjorth & Williams (2010) for a further discussion of the problems with the Lynden-Bell’s approach and proposed solutions.)

Hjorth & Williams (2010) argue that to apply statistical mechanics to collisionless self-gravitating systems requires one to make two important modifications to the Lynden-Bell (1967) approach. First, the proper state space for collisionless systems, like dark matter halos and stars in elliptical galaxies, is energy space and not the standard phase-space. The rationale being that in a collisionless system in equilibrium the particles’ energies are fixed, so using energy space automatically ensures collisionlessness. Second, the expression for the possible number of states, or entropy, involves  $n!$ , where  $n$  is the occupation number in energy space. When extremizing entropy, it is customary to simplify  $\ln n!$  using the Stirling approximation, which is valid only for large  $n$ . Hjorth & Williams (2010) replace the Stirling approximation

with an expression that treats all  $n$  regimes very accurately; the implication being that low  $n$  regime, where  $n$  is 0, 1, 2, ... is relevant in self-gravitating systems. With these two modifications they derive the most likely distribution in energy for the equilibrium systems,

$$N(E) \propto \exp(-\beta[E - \Phi_0]) - 1 = \exp(\phi_0 - \epsilon) - 1. \quad (4)$$

DARKexp is a single parameter family of models, with  $\phi_0$  acting as a dimensionless potential depth. Density profiles based on DARKexp models can be found in Williams & Hjorth (2010). Unlike isothermal spheres, DARKexp systems have finite mass and energy. A comparison with the results of collisionless dark matter simulations are presented in Williams et al. (2010). The simulations are a very good match to DARKexp models with  $\phi_0$  around 4-5.

We emphasize that both collisional and collisionless systems, as described by the Madsen and DARKexp models, can be derived as the most likely statistical states. Aside from this, Madsen and DARKexp models have one other important feature in common: their derivation requires that the low occupation number regime is treated properly. The reason why this is the case for self-gravitating systems, while the Stirling approximation is adequate for other physical systems, is not yet definitively decided. What we can say is that realistic gravitationally bound systems have DFs that are truncated, leading to regions of state space that are very sparsely populated. It is therefore not surprising that entropy calculations, which depend on counting available energy states, require those sparsely populated regions to be accurately accounted for.

### 3.3 Our goals

The primary goal of this paper is to find out whether GCs are better fit by King or DARKexp density profiles. These are both “first principles” models and not empirical fitting functions like the Wilson and power-law models. If a first-principles model is shown to fit the mass distribution of GCs, the most straightforward conclusion is that the physics that went into making the model applies to GCs. However, it is also possible that the goodness of fits is purely fortuitous, i.e. a complex combination of diverse dynamical effects happen to make the model a good fitting function.

Our secondary goal concerns only those clusters that are well fit by the King model. Recall that the King and Madsen DFs differ somewhat because one is continuous and the other is discrete. It is not *a priori* obvious which one is appropriate for physical systems. The resulting King and Madsen density profiles are very similar, but not identical, so it makes sense to ask which of the two is preferred by real self-gravitating collisional systems.

## 4 DATA

Noyola & Gebhardt (2006) present the largest homogeneous set of non-parametrically estimated surface brightness (SB) profiles of 38 Galactic globular clusters. The inner regions of the profiles are derived from archival HST WFPC2 images, while the outer profiles are obtained from ground-based observations. Estimating an unbiased smooth SB profile of the inner portions of GCs is not trivial, because a small number

of very bright giant and horizontal branch stars introduces a considerable amount of shot noise. NG06 performed several simulations to determine the optimal way of overcoming shot noise, as well as photon noise. After extensive testing on synthetic data, they conclude that a certain combination of subtraction and masking of bright stars works best in recovering their input profiles. The profiles of the outer radial regions were taken directly from Trager et al. (1995), who used Chebychev polynomial fits to the photometric points of ground-based data. The analysis of NG06 combines the HST and ground-based data into continuous composite profiles of 38 clusters, which range from 2.36 to 3.68 decades in radius. For each cluster they publish 100 data points, spaced equally in  $\log(r)$ .

The objectives of Noyola & Gebhardt (2006) were to estimate the central SB slope of GCs, deproject the light of GC where possible, and estimate the central slope of the 3D light distribution. Hence, they derive uncertainties on the inner slope, but do not quote errors for the full radial range of the SB profile. It is probably reasonable to assume that the typical uncertainties in SB over the whole radial range are smaller than those in the individual HST data points, which are  $\sim \pm 0.15$  mag/arcsec<sup>2</sup>. In this paper we calculate *rms* differences between NG06 fits and our theoretical models, and so do not use data uncertainties. Our *rms* values span the range from  $\sim 0.014$  to  $\sim 0.8$  mag/arcsec<sup>2</sup> (see Table 1), which can be compared to the above quoted approximate uncertainty.

## 5 FITTING GC SURFACE BRIGHTNESS WITH DARKEXP AND KING MODELS

Dynamical studies of GCs are consistent with them having no dark matter. The main source of radial  $M/L$  variation in GCs is mass segregation. Even in the presence of mass segregation, radial  $M/L$  variations need not be large. Lane et al. (2009, 2010) find only small radial variations in  $M/L$  in their GC sample. In the radial range that the authors consider trustworthy their estimate of  $M/L$  varies by less than a factor of 1.5–2, and is consistent with being constant. Furthermore, the Noyola & Gebhardt (2006) procedure of obtaining smooth SB profiles relies mostly on main sequence stars, and so minimizes the effects of mass segregation. In this work we assume that  $M/L$  is constant with radius, and hence the shape of the SB profiles gives the shape of the radial mass distribution in these systems. One has to keep in mind that this is an approximation, and the true  $M/L$  must have some radial dependence.

We use the non-parametrically smoothed profiles of NG06 as our input. We fit the SB of each Globular Cluster with 2D projected DARKexp and King models. DARKexp models are characterized by a single shape parameter,  $\phi_0$ , a dimensionless potential depth. King models are also characterized by a single shape parameter,  $\Phi(0)/\sigma^2$ , a dimensionless combination of central potential and system’s constant velocity dispersion. An alternate parameterization is through the concentration parameter,  $c_K \equiv \log(r_{tidal}/r_{core})$ ; there is a monotonic relation between  $\Phi(0)/\sigma^2$  and  $c_K$  for King models.

DARKexp models have a simple analytical expression for the energy distribution  $N(E)$ , and King models have a

simple expression for the distribution function,  $f(E)$ . However, neither model has an analytical expression for the corresponding density profiles, so these have to be obtained numerically, even for isotropic systems. We first calculate a library of DARKexp and King models and then compare them to the input profiles from NG06.

Our fitting is done in the space of  $\log(\text{SB})$  vs.  $\log(r)$ , not the corresponding linear quantities, and the *rms* deviations between GCs and models are also calculated in the log space. While DARKexp and King models are one parameter families, we fit for three parameters, one shape parameter, and radial and SB normalizations. We use the full radial range for all 38 clusters presented in NG06, and give each of their 100 points equal weight.

Table 1 presents our results. The core collapse status of the cluster is denoted by the labels *c* (collapsed) and *c?* (possibly collapsed), and were taken from NG06. In general, a cluster is classified as core collapsed if it has a cuspy, or steep SB profile extending to the center (Meylan & Heggie 1997). In this paper we label clusters *c* and *c?*, but make no judgement as to their physical state. The second and third sets of columns, separated by vertical lines, show the DARKexp and King model fit parameters. DARKexp  $\phi_0$  and King  $\Phi(0)/\sigma^2$  and  $c_K$  are described above. In order to compare the two models directly, we have defined a new concentration parameter,  $c_{D13}$  and  $c_{K13}$  as  $c_{13} = \log[r(\gamma = 3)/r(\gamma = 1)]$ . These concentration values are also shown in the Table. Next to the *rms* values for each of the two models, we quote, in parentheses, the separate *rms* for the inner and the outer regions of the radial profile. These regions each contain 50 of the total 100 points presented in NG06. These *rms* values are evidence that neither the inner nor the outer portion of the fit dominates the total *rms*.

Figures 2 and 3 summarize our fits for DARKexp and King models, respectively. The horizontal axis is the potential depth (shape parameter) of the model, and the vertical axis is the *rms* of the fit. The best-fit model for each of the 38 clusters is represented by a solid dot, which is circled if the cluster is considered to be core collapsed. The best fits for individual clusters are shown in Figures 4-13. Red dashed curves are the NG06 data, blue curves are best-fit DARKexp, and black are best-fit King profiles. The fit residuals (in  $\Delta \text{ mag/arcsec}^2$ ) are shown in the bottom insets of each panel. Note that some residual curves show small amplitude fluctuations with radius, that look like noise. These come from the NG06 surface brightness data which is quoted to only 4 significant digits. This limited precision shows up as ‘noise’, which is especially visible when the fits are good. We do not smooth over this noise here, but do smooth over it in Section 8.

All results presented in this Section indicate that most clusters are better fit by DARKexp than King. Additionally, about a quarter of the clusters are fit very well, over the entire available radial range, by DARKexp. Figure 14 plots best-fit *rms* of DARKexp and King models; only eight clusters are better fit by King. Note that all eleven core collapse GCs are better fit by DARKexp than King models. Even if these are taken out, there is still a clear preference for DARKexp for non-core collapse GCs. Recall that the DARKexp model was built to reproduce the equilibrium states of collisionless systems, like dark matter halos. Apparently, many GCs are also well fit by it. We interpret this

result to mean that the overall SB profiles of GCs may be less affected by collisional processes among its member stars than previously assumed.

To further compare DARKexp and King fits, in Figure 15 we show residuals from best-fits for all 38 clusters, for DARKexp (top panel) and King (bottom panel), respectively. The horizontal axis is normalized by the core radius of each cluster, which was defined by NG06 as the radius where the SB drops to half its central value. Note that this core radius definition is non-parametric and thus unrelated to the definition of the core radius in King models; the half-light radius was determined from non-parametric smoothed profiles. In addition to showing that DARKexp residuals are smaller, the figure also suggests that the King residuals show a systematic pattern, while DARKexp residuals are more random. If true, then this is an additional indication that DARKexp are a better fit, at least typically, than King models.

A skeptic might argue that the full radial range of a GC should not be fit with a single profile because different dynamical processes are at play at small and large radii. The innermost radii might be affected by a central black hole, or core collapse and compact binaries, while the outermost radii may be populated by extra-tidal stars which are not in equilibrium with the global potential. We do not address these possibilities, aside from pointing out that these modifications would need to be described by multiple adjustable parameters.

Before proceeding, we examine one more issue relevant for fitting, the radial extent of the data. The goodness of fit depends on the radial range being fit, and we have already mentioned that the shorter ranges available in the 1970’s and 1980’s were well modeled by the King profile. In Figure 16, the vertical axis shows the log of the ratio of the radial range given in NG06, and the horizontal axis the *rms* of the best-fit: solid dots represent DARKexp and empty triangles, King. The vertical solid and dashed lines in the top and bottom halves of the plot show the average *rms* for the DARKexp and King fits, respectively. As expected, a larger radial range leads to poorer fits for both models. DARKexp is moderately better than King for smaller radial ranges (bottom half of the plot). As the radial range gets larger (top half of the plot), DARKexp fits become noticeably better fits than King. This too points towards DARKexp being a better descriptor of GCs.

## 6 KING VS. MADSEN MODELS

Our secondary goal in this paper is to compare King (1966) and Madsen (1996) models. The King and Madsen models are created by smooth and discrete distribution functions, respectively, and show corresponding differences in the density profiles. Since it is not clear which of these two are more physically appropriate, we fit both models to twelve GC that are well fit,  $rms < 0.15$ , by King models (except NGC 6352, see the caption of Figure 3). The clusters that are poorly fit by King tend to be much better fit by DARKexp (see Figure 14), and so are unlikely to be better fit by the Madsen model.

Figure 17 presents the results. The blue solid and dashed lines, and the solid and empty circles represent King

and Madsen fits, respectively. The best fits for the same cluster are connected by a red straight line segment. Eleven of the twelve clusters are better fit by the King model. Because the differences between King and Madsen profiles are small, we might have expected a breakdown closer to 50/50. The reason is probably the very sharp drop off in density that Madsen models have at large radii, a consequence of the discreteness of the distribution function at low occupation numbers. Real GCs do not show such steep drop off.

## 7 DARKEXP VS. KING MODELS: A CLOSER LOOK AT SOME GCs

In this Section we consider a few specific GCs and compare the standard description of their SB to the one using DARKexp.

Modern data, especially HST and ground-based composite data sets such as the one provided by Noyola & Gebhardt (2006), have extended radial coverage and good resolution down to very small radii. Here we illustrate, with one specific example, that a large radial range is often needed to discriminate between competing models. Consider NGC 6388, the cluster with the largest velocity dispersion,  $\sigma = 18.9$  km/s (Pryor & Meylan 1993) in the NG06 sample. Using data spanning  $3''$  to  $250''$ , Illingworth & Illingworth (1976) fit a King model of  $c_K = 1.75$ . Within these 2 radial decades, the King model fits the data well. If we truncate the NG06 data to the above radial range, our best-fit King model has  $c_K = 1.77$ , consistent with earlier findings. However, the full 3.14 radial decades clearly prefer DARKexp over King (Figure 9), with  $rms$  values of 0.062 and 0.455, respectively.

About 20% of Galactic GCs show deviations from King models by having steeper central SB profiles, *i.e.*, cusps instead of cores. Moderately steep central cusps could be, in some cases, a signature of an intermediate mass black hole (IMBH), between  $10^2$  and  $10^4 M_\odot$  (though the presence of a shallow cusp is not a reliable indication of the IMBH; Vesperini & Trenti 2010). Steeper cusps are explained as post-core collapse clusters. However, as NG06 point out, clusters undergoing gravothermal oscillations should spend a small fraction of their lives in collapsed states. If all clusters that show cusps are assumed to be in a collapsed state, then we are catching a disproportionately large fraction of GC in this short-lived phase of their evolution. Consider the GC with the steepest cusp in the NG06 sample, NGC 6681 (M 70). The King fit has  $c_K = 2.3$  and  $rms = 0.194$ . The DARKexp fit has  $\phi_0 = 7.5$  and  $rms = 0.065$ . The rather steep central cusp is very well accommodated by DARKexp. Whether it speaks for or against the cluster being core collapse or hosting a central black hole is not clear, but the overall mass distribution over the entire 2.72 decades in radius is definitely better accounted for by DARKexp.

Another example is NGC 6715 (M 54). Ibata et al. (2009) find density and velocity dispersion cusps within the central 0.3pc which they interpret as evidence of a  $9400 M_\odot$  IMBH. However, they can also explain the cusp if the central stars have moderate radial anisotropy. Wrobel et al. (2011) find no evidence for the IMBH in the X-rays, deriving an upper limit on the Eddington ratio  $< 1.4 \times 10^{-10}$ . Regardless of whether the cluster hosts an IMBH, DARKexp provides

a better fit, including the central cusp, than King; the two  $rms$  are 0.104 and 0.595, respectively.

Deviations from King models at large radii are also seen. These are generally attributed to extra-tidal stars, since GCs are expected to lose stars due to tidal stripping. Several GCs do show spectacular tidal tails. However, in some others, the ‘extra-tidal’ distribution is circularly symmetric, and hence at odds with a tidally induced scenario. Such a distribution can be explained by evaporated stars (Küpper et al. 2010, 2011). However, a DARKexp model also fits. For example, NGC 5694 was recently examined by Correnti et al. (2011) using VIMOS/VLT. These authors note that they do not see a break, or any tidal tails beyond the cluster’s tidal radius of 3.15 arcmin. Instead, the stellar distribution smoothly continues across the tidal radius, up to 10 arcminutes from the center. It shows an almost constant SB slope before and after the tidal radius, which the authors fit with a power law,  $R^{-3.2}$  (see their Figure 3). In 3D this would be  $r^{-4.2}$ , completely consistent with DARKexp, which has an asymptotic outer slope of  $-4$ , independent of  $\phi_0$ . Our best-fit DARKexp model for NGC 5694 has  $\phi_0 = 1.75$ , with  $rms = 0.076$ , compared to King model  $rms = 0.163$ .

That truncation radii based on King model fitting may not correspond to tidal truncation due to the Galaxy is generally acknowledged. In Figures 4-13 the empty downward triangles indicate the King model truncation radii taken from Gnedin & Ostriker (1997). The filled triangles indicate the truncation radius estimated from the strength of the Galactic tidal field,  $r_t^3 = r^3(M_{GC}/[3M(<r)])$ , where  $r$  is the Galactocentric distance,  $M_{GC}$  is the GC’s mass obtained from its absolute luminosity in  $V$  and a constant mass-to-light ratio of  $M/L = 2.5$  in solar units, and  $M(<r)$  is the mass of the Galaxy interior to the current (*i.e.* not pericenter) location of the cluster. (Note that some truncation radii lie outside the limit of the figures.)

Some GCs that are not well fit with King models and show signs of mass segregation are fit with multi-mass King models; see for example, Da Costa & Freeman (1976). These more complex models are especially needed for clusters that cover a larger dynamic range in SB, up to 5 decades. NGC 5272 (M3) is one example. Da Costa & Freeman (1976) show that the inner radial range can be fit with  $c = 1.29$  King, while the outer with  $c = 1.98$ . Their actual fitted model has 10 mass ranges, for the data that span 2.4 decades in radius. NG06 data spans 3.6 decades, and the DARKexp fit has  $rms = 0.211$ , which appears comparable to the residuals of the 10-mass King profile (see Fig 3 of Da Costa & Freeman (1976)).

An illustration of how different estimates of global parameters can be depending on the model fitted, we quote effective radii and enclosed mass for two representative clusters, which also happen to be the first two in Table 1. In the case of NGC 104, DARKexp and King models fit about equally well, while NGC 1805 is much better fit with DARKexp. First, we note that we use half-mass radii instead of core radii because the latter are not defined for DARKexp models. Further, because the outer-most projected density profile of DARKexp falls off as  $r^{-3}$ , the mass enclosed scales as  $M(<r) \propto r^{-1}$ . This relatively slow fall-off makes ‘total’ mass a radius-dependent quantity, and requires one to decide where to truncate the DARKexp to calculate the ‘total’ mass. We chose to use the last NG06 data point. With

these choices, the ratio of the half-mass radii of best-fit models for NGC 104 is  $R_{\text{DARKexp}}/R_{\text{King}} = 0.95$ , and the ratio of total masses is  $M_{\text{DARKexp}}/M_{\text{King}} = 1.0$ . For NGC 1851, the corresponding values are both 0.77.

## 8 FITTING 3D LIGHT DISTRIBUTION OF GCC WITH DARKEXP AND KING MODELS

Of the 38 GC in the Noyola & Gebhardt (2006) set, 12 show central dips in the smooth non-parametric fits, and cannot be deprojected to yield 3D density profiles. For the remaining 26 clusters, NG06 present their non-parametric deprojections. We take these 26 GCs, smooth them to eliminate the fluctuations due to the finite precision of their published results (see the sixth paragraph of Section 5 above), and compute 3D density slope,  $\gamma$ . These are plotted in Figure 18. For reference, we also plot five DARKexp and four King models, with  $\phi_0 = 5.66, 4.0, 2.83, 2.0, 1.0$  and  $c_K = 0.84, 1.25, 1.83, 2.35$ , respectively. These particular values for  $\phi_0$  and  $c_K$  were chosen arbitrarily.

Figure 18 is another way of looking at the same GC data. The 26 clusters are grouped by their DARKexp  $rms$  values, with the top left panel showing the 7 GCs which are fit by DARKexp very well, while the bottom right panel shows 6 GCs where DARKexp is a relatively poorer fit. Note that the bulk of the clusters have shallow inner density slopes, though in most cases these are not as shallow as those of King cores. DARKexp, on the other hand, has a range of slopes and slope derivatives at  $r < r_{-2}$  that match GC well. At  $r > r_{-2}$  some clusters are consistent with DARKexp profiles, but a few show non-monotonic  $\gamma$  behavior reminiscent in character of King profiles. Overall, even though DARKexp provide better fits, similarities with King density profiles are also seen at some radii.

## 9 CONCLUSIONS

King (1966) models, which are based on the assumption of two-body collisional dynamics (Madsen 1996), do not provide good fits to surface density profile of many Globular Clusters, especially those whose data span a large radial range. Deviations occur at small and large radii, which are usually explained by physics beyond the King model. Motivated by these widespread departures, we ask if collisionless effects due to collective behavior of cluster stars could be important. In Section 2, we present two independent order-of-magnitude arguments that answer the question in the affirmative.

We then use previously created Globular Cluster surface brightness profiles to further test the relevance of collisionless effects. Our goal is made easier because there exist first-principles analytical models of collisional and collisionless systems, the King-Madsen and the DARKexp models, respectively. Both were derived based on maximum entropy statistical arguments. Both are one parameter families, and can be readily converted to density profiles and hence compared to the surface brightness profile of GCs (assuming GCs contain no dark matter and have constant mass-to-light ratios). We take the SB profiles from the work of Noyola &

Gebhardt (2006) who present smooth non-parametric composite profiles based on HST and ground-based data and fit these with King, Madsen, and DARKexp density profiles.

Our main finding is that DARKexp models fit considerably better than either King or Madsen models, over the entire available radial range. While this is not proof that collisionless dynamics has shaped the mass distribution of GCs, it does suggest it as an interesting possibility. It is already well known that the consequences of collisional processes, like the presence and hardening of binaries, mass segregation and evaporation of stars are important in observed and simulated clusters (Meylan & Heggie 1997). In this paper we demonstrate that the overall density profile is well described by a collisionless prediction, the DARKexp family of models. Taken together, these observations suggest that collisional and collisionless processes co-exist in GCs, but are responsible for different sets of properties. An alternative explanation is that a good DARKexp fit is purely fortuitous in that it allows for a cuspy central profile and so phenomenologically accounts for the effects of  $M/L$  variation with radius as well as the effects of core collapse or post core collapse, etc., but the physics is not related to collisionless relaxation; DARKexp just happens to be a better fitting function to a very complex system.

Because King models are apparently not the best ‘typical’ model for GC, we caution against using these to derive cluster global structural parameters, like characteristic radii and enclosed mass, especially if these are used in other types of analyses, for example, to look for correlations with metallicity, colors, age, etc.

A secondary question we have addressed concerns an intriguing property of self-gravitating systems. The derivation of Madsen and DARKexp models is based on statistical mechanics; basically counting the number of particles in various states. In classical applications, all states have large occupation numbers, so the Stirling approximation is commonly used. Madsen and DARKexp models depend critically on the accurate treatment of the low occupation number regime and so raise the question of how the DF should behave when  $n = 1, 2, 3, \dots$ . Should it be step-like, i.e. discrete, or should it be smooth? Madsen (1996) and King (1966) models are the two corresponding versions. (DARKexp is smooth.) A comparison of Madsen and King models for a subset of GCs shows the latter fit better.

In the future it will be interesting to extend our analysis to include the dynamical information on Globular Clusters. Velocity dispersion profiles, though of poorer quality and of shorter radial range than surface brightness profiles, are available for some clusters, and can be used in combination with the surface brightness profiles to assess the state of the GCs (Zocchi et al. 2012).

Since DARKexp has already been shown to fit the results of collisionless dark matter  $N$ -body simulations quite well (both in the density,  $\rho(r)$  and energy space,  $N(E)$ ; Williams et al. 2010), it is interesting to compare the best-fitting shape parameter,  $\phi_0$ , to those obtained in this work for GCs.  $N$ -body generated dark matter halos have a narrow range of  $\phi_0$  around 4–5. GCs (excluding those that are poorly fit by DARKexp) mostly have  $\phi_0$  between 1 and 3, because at appropriate radii these DARKexp profiles have shallow, or flat density slopes. A few GCs have  $\phi_0$  values

between 3 and 8. It is unclear why these values of  $\phi_0$  are preferred in either one of the systems.

The Dark Cosmology Centre is supported by the Danish National Research Foundation. LLRW thanks Evan Skillman for valuable suggestions.

## REFERENCES

- Barnes, E.I. & Williams, L.L.R. 2012, *ApJ*, 748, 144  
 Baumgardt, H. & Makino, J. 2003, *MNRAS*, 340, 227  
 Binney, J., Tremaine, S. 1987, *Galactic Dynamics*, (Princeton, NJ:Princeton)  
 Carballo-Bello, J.A., Gieles, M., Sollima, A., Koposov, S., Martinez-Delgado, D. & Penarrubia, J. 2012, *MNRAS*, 419, 14  
 Correnti, M., Bellazzini, M., Dalessandro, E., Mucciarelli, A., Monaco, L. & Catelan, M. Preprint, arXiv:1105.2001  
 Da Costa, G. S. & Freeman, K. C. 1976, *ApJ*, 206, 128  
 Elson, R. Hut, P. & Inagaki, S. 1987, *ARA&A*, 25, 565  
 Gnedin, O.Y. & Jeremiah P. Ostriker, J.P. 1997, *ApJ*, 474, 223  
 Hjorth, J. & Williams, L.L.R. 2010, *ApJ*, 722, 851  
 Ibata, R. et al. 2009, *ApJ*, 699, L169  
 Illingworth, G. & Illingworth, W. 1976, *ApJS*, 30, 227  
 King, I.R. 1966, *AJ*, 71, 64  
 Kalirai, J. S. et al. 2007, *ApJ*, 657, L93  
 Küpper, A.H.W., Mieske, S. & Kroupa, P. 2011, *MNRAS*, 413, 863  
 Küpper, A.H.W., Kroupa, P., Baumgardt, H. & Heggie, D.C. 2010, *MNRAS*, 407, 2241  
 Lane, R. R., Kiss, Laszlo L., Lewis, G. F., Ibata, R. A., Siebert, A., Bedding, T. R. & Szekely, P. 2010, *MNRAS* 401, 2521  
 Lane, R. R., Kiss, Laszlo L., Lewis, G. F., Ibata, R. A., Siebert, A., Bedding, T. R. & Szekely, P. 2009, *MNRAS*, 400, 917  
 Lynden-Bell, D. 1967, *MNRAS*, 136, 101  
 Madsen, J. 1996, *MNRAS*, 280, 1089  
 McLaughlin, D.E. & van der Marel, R.P. 2005, *ApJ*, 161, 304  
 Merritt, D. 2005, "Nonlinear Dynamics in Astronomy and Physics, A Workshop Dedicated to the Memory of Professor Henry E. Kandrup", ed. J. R. Buchler, S. T. Gottesman and M. E. Mahon  
 Meylan, G. & Heggie, D.C. 1997, *A&A Rev*, 8,1  
 Michie, R.W. 1963, *MNRAS*, 125, 127  
 Noyola, E. & Gebhardt, K. 2006, *AJ*, 132, 447 (NG06)  
 Ogorodnikov, K. F. 1957, *Soviet Astronomy*, 1, 748  
 Pryor, C. & Meylan, G. 1993, *APS Conf. Series*, Vol. 50, 357, eds. S.G. Djorgovski and G. Meylan  
 Simons, S. 1994, *Am. J. of Phys.*, 62, 515.  
 Spitzer, L. 1987, "Dynamical Evolution of Globular Clusters" (Princeton: Princeton Univ. Press)  
 Stephens, A.W., Catelan, M. & Contreras, R.P. 2006, *AJ*, 131, 1426  
 Trager, S.C., King, I.R. & Djorgovski, S. 1995, *AJ*, 109, 218  
 van den Bergh, S. 2011, *PASP*, in press  
 Vesperini, E. & Trenti, M. 2010, *ApJL*, 720, L179  
 Williams, L.L.R. & Hjorth, J. 2010, *ApJ*, 722, 856  
 Williams, L.L.R., Hjorth, J. & Wojtak, R. 2010, *ApJ*, 725, 282  
 Wilson, C.P. 1975, *AJ*, 80, 175  
 Wrobel, J.M., Greene, J.E. & Ho, L.C. 2011, 1107.4583  
 Zocchi, A., Bertin, G. & Varri, A.L. 2012, *A&A*, accepted



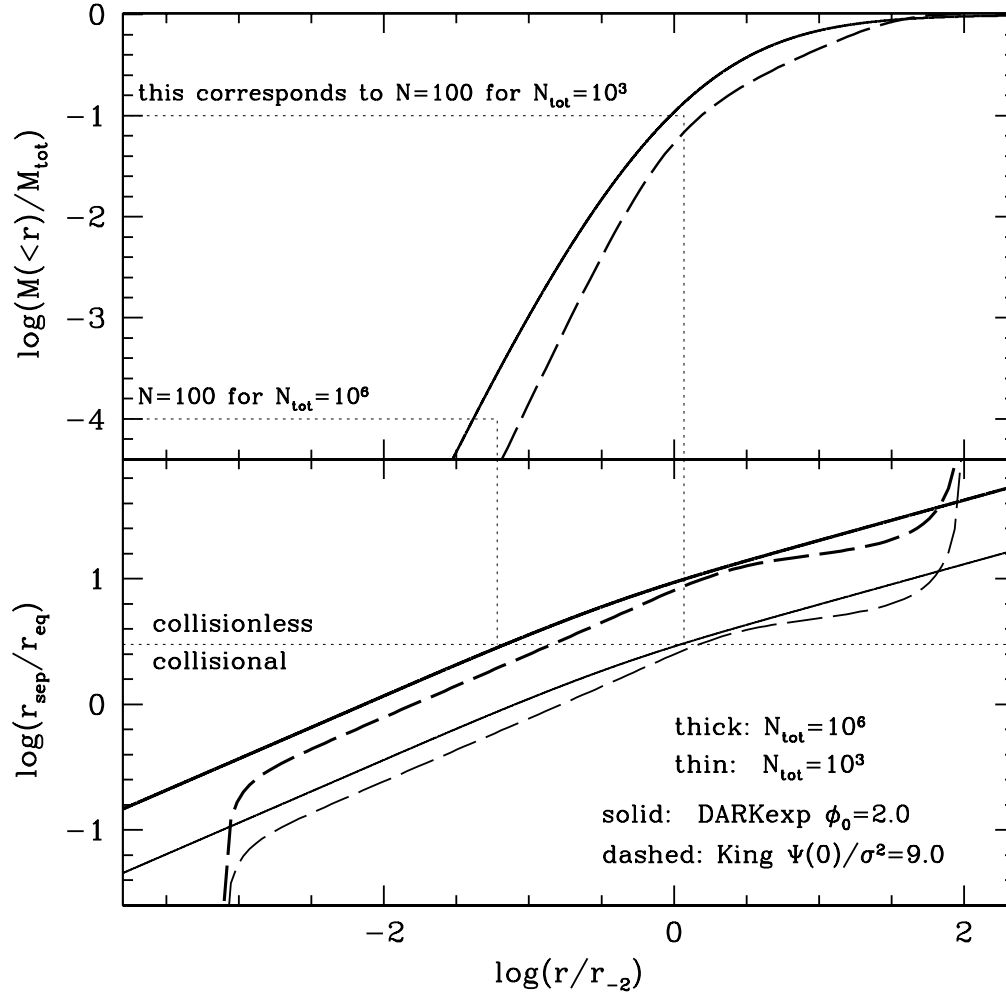


**Figure 1.** A comparison of two order of magnitude collisionality tests: top panel is based on  $t_{dyn}$  and  $t_{2bd}$  time-scales, bottom panel is based on length-scales. The two estimates agree. See Section 2 for details.

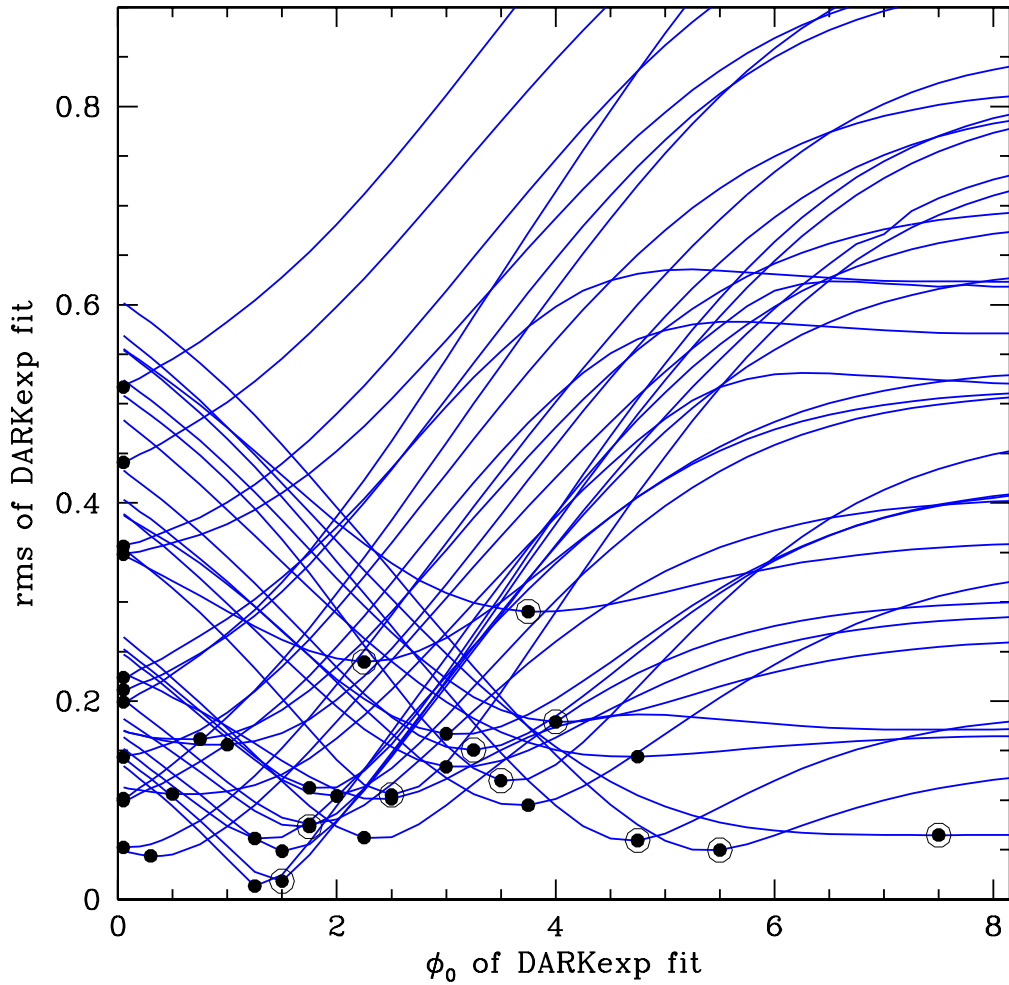


**Figure 2.** The curves represent DARKexp fits to 38 GCs. The best-fit DARKexp model for each cluster is marked by a solid dot. Eleven clusters have best-fit  $\phi_0 = 0.05$ ; these are not to be trusted because 0.05 was the smallest  $\phi_0$  value considered because the outer SB profiles of most of these clusters are steeper than what DARKexp can have, so no DARKexp model can provide a good fit. The circled dots represent core collapse GC.

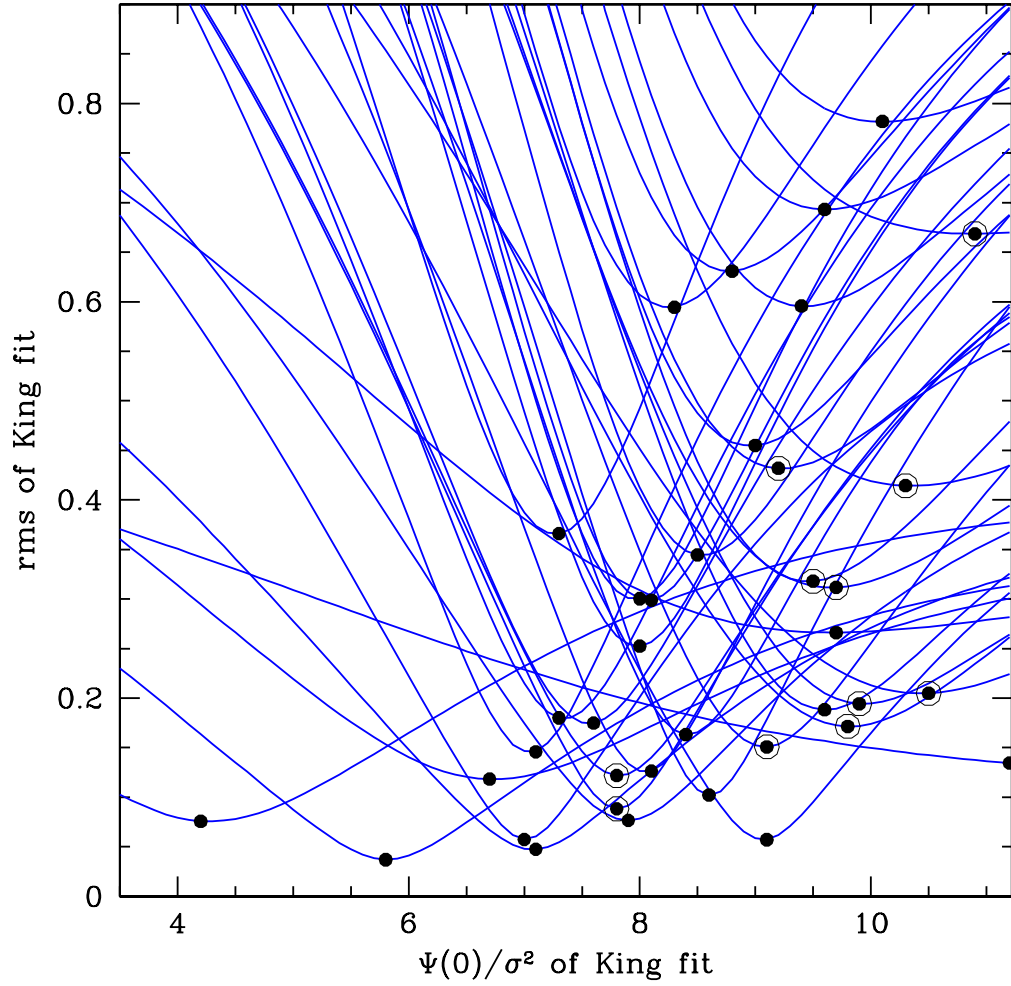


**Figure 3.** Similar to Figure 2, but for King fits. The cluster with best-fit  $\Psi(0)/\sigma^2$  beyond 11 (at the right edge of the plot) is NGC 6352; Figure 9. It has an upturn in SB at large radii, which is difficult to fit even with very large concentration King models.

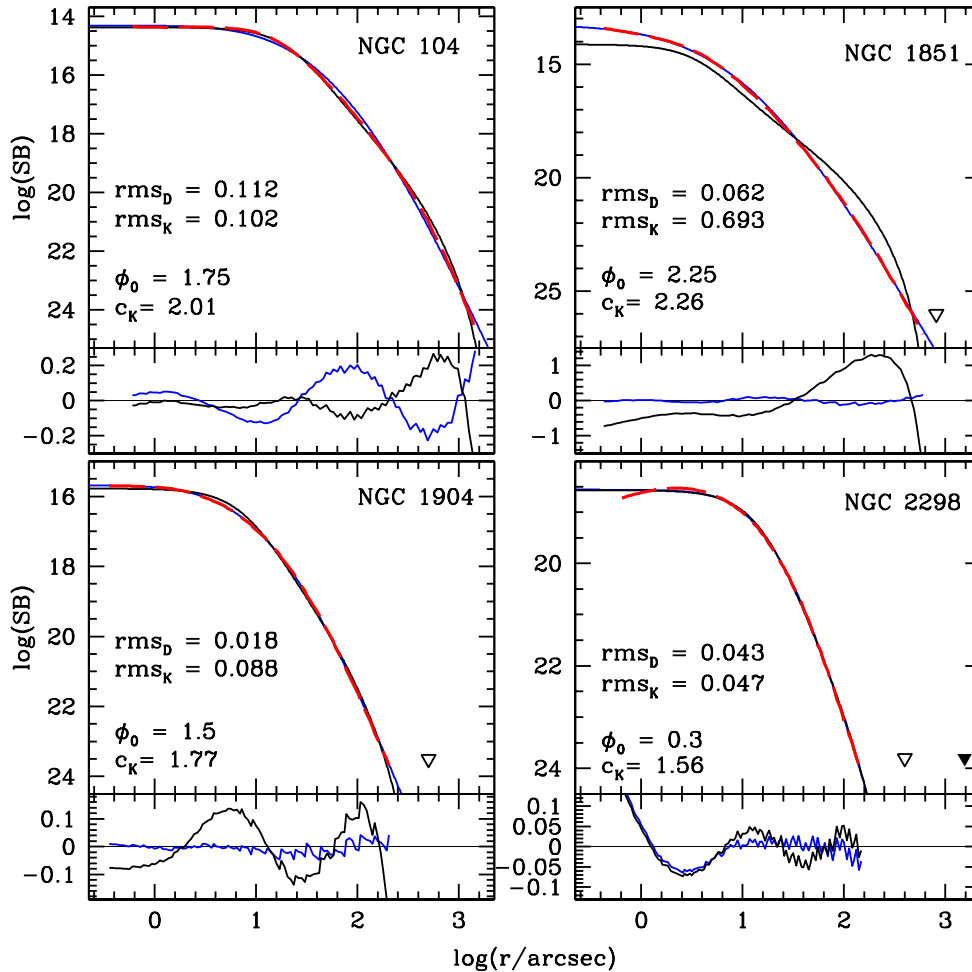


**Figure 4.** DARKexp (blue) and King (black) best-fits to four GCs. The red dashed curve is the Noyola & Gebhardt (2006) data, which consists of HST and ground-based observations, jointed and smoothed by those authors. The surface brightness (SB) is in  $\text{mag}/\text{arcsec}^2$  in the  $V$  band. The  $\text{rms}$  between the data and models are indicated in the plot, together with the values of the dimensionless potential depth for DARKexp model,  $\phi_0$ , and the King concentration parameter,  $c_K$ . The fit residuals are shown in the bottom insets. The vertical scale is the difference in SB, in  $\text{mag}/\text{arcsec}^2$ ; the its span varies between panels. The empty downward triangles indicate the King model truncation radii taken from Gnedin & Ostriker(1997). The filled triangles indicate the truncation radius estimated from the strength of the Galactic tidal field; see Section 7.

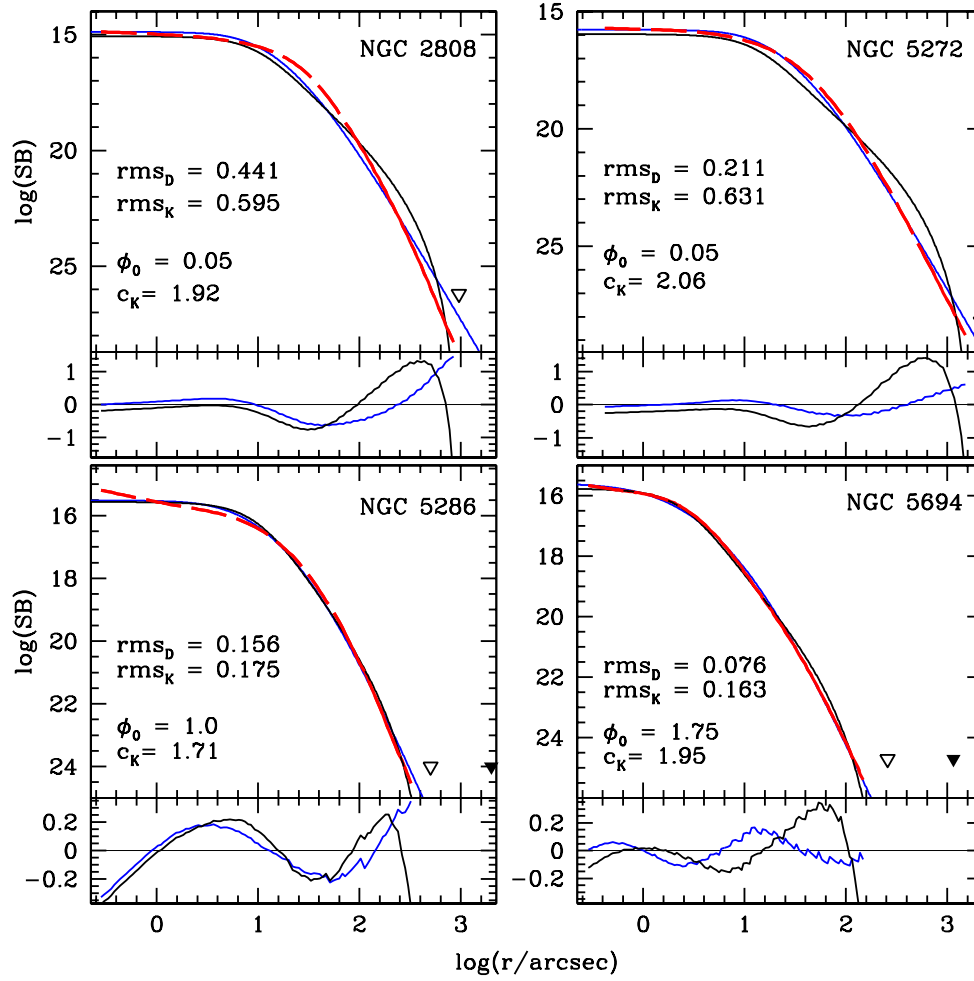


Figure 5. Similar to Figure 4.

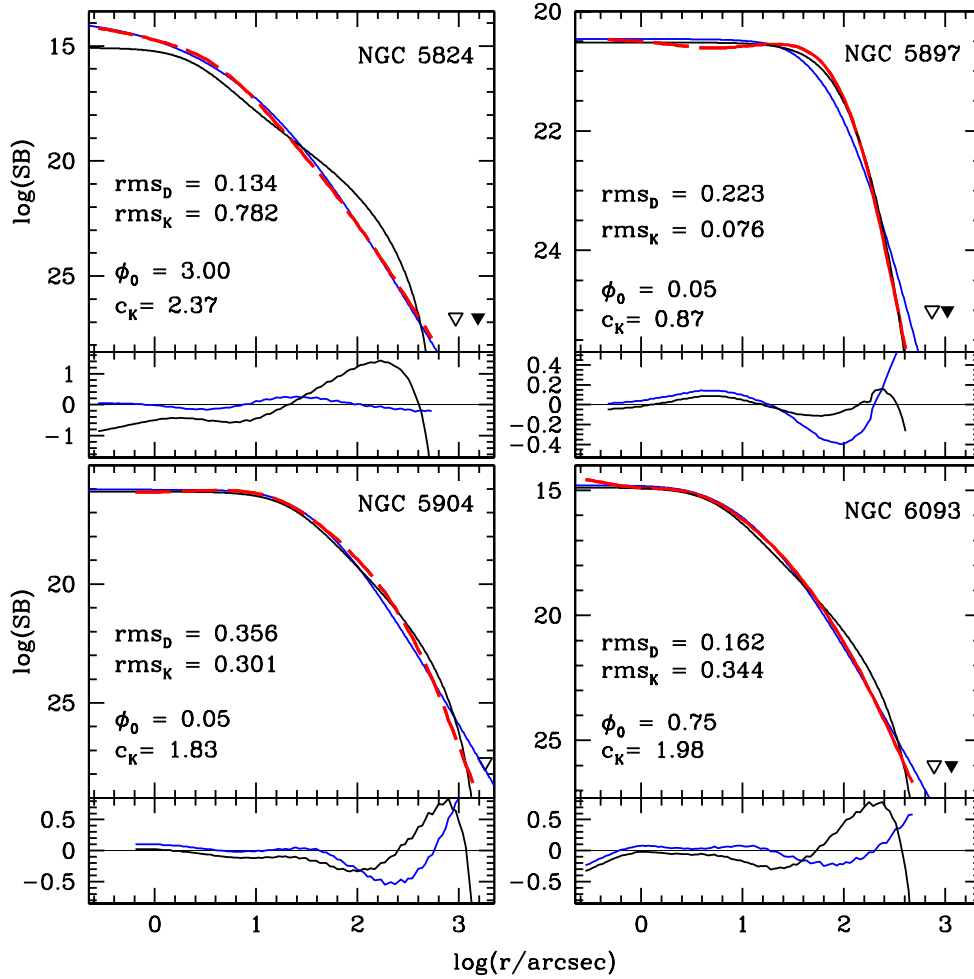


Figure 6. Similar to Figure 4.

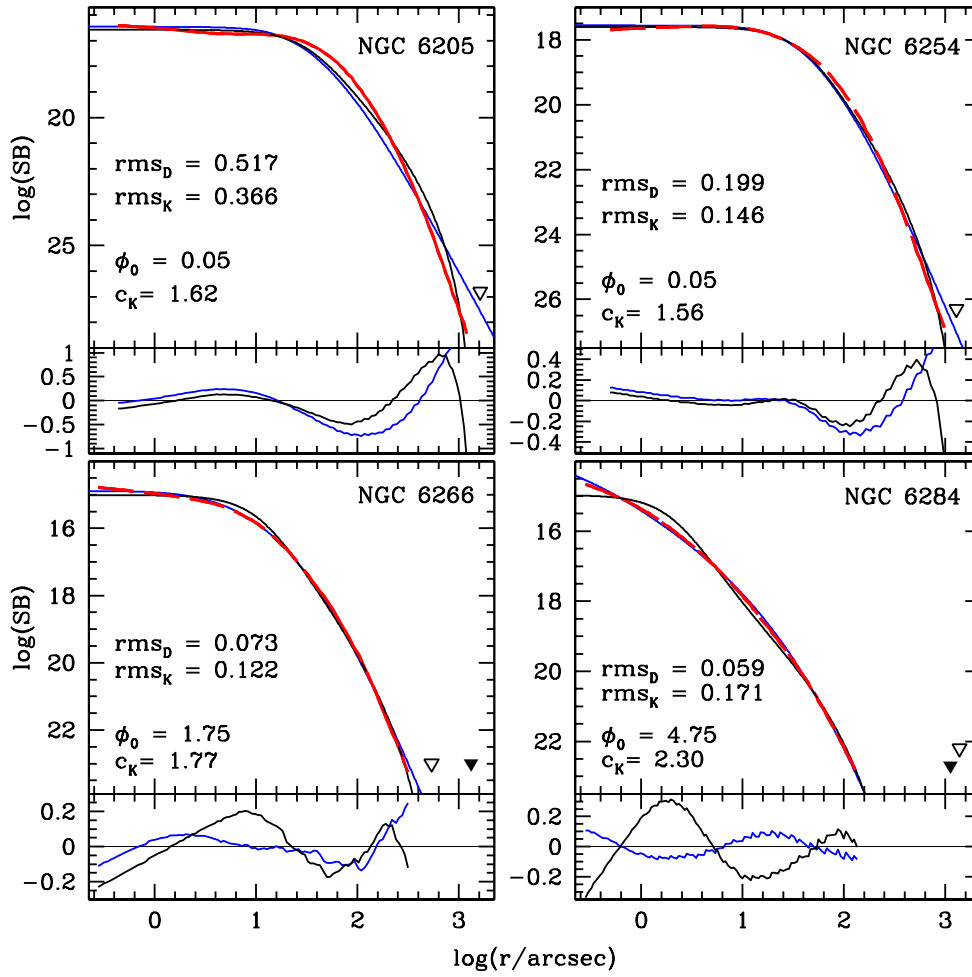


Figure 7. Similar to Figure 4.

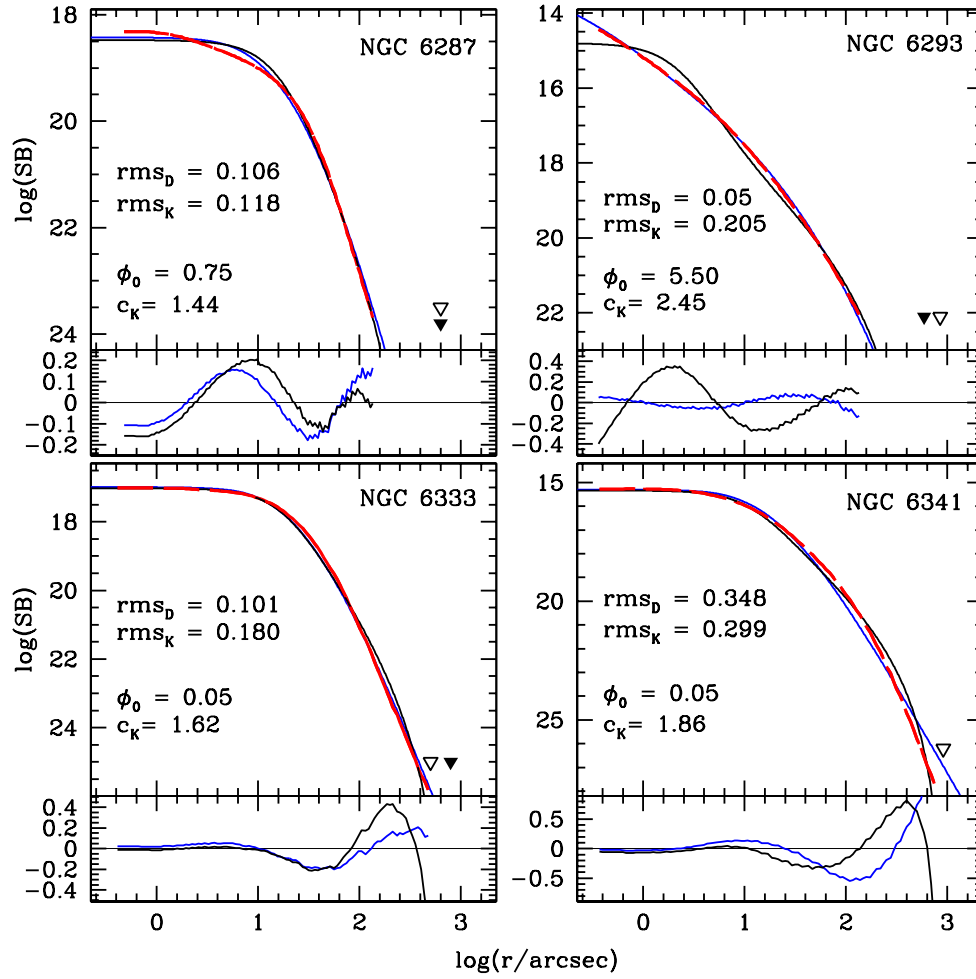


Figure 8. Similar to Figure 4.



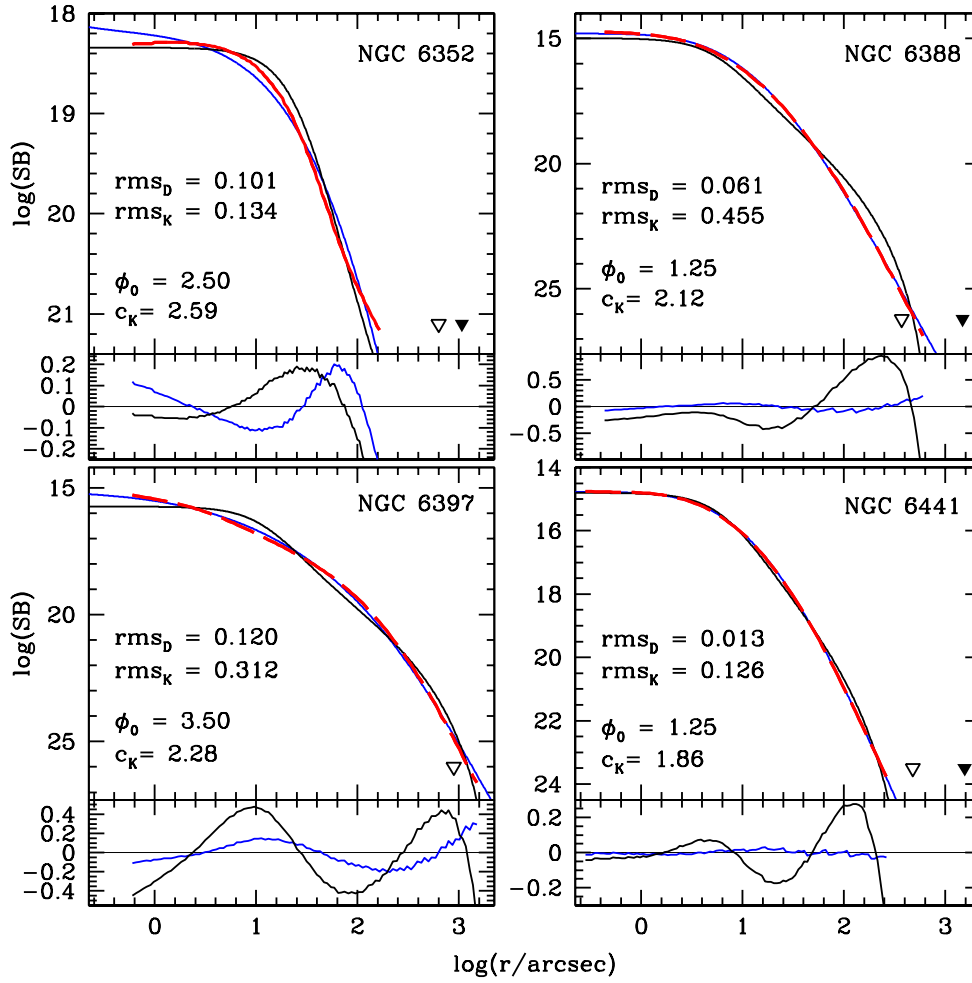


Figure 9. Similar to Figure 4.

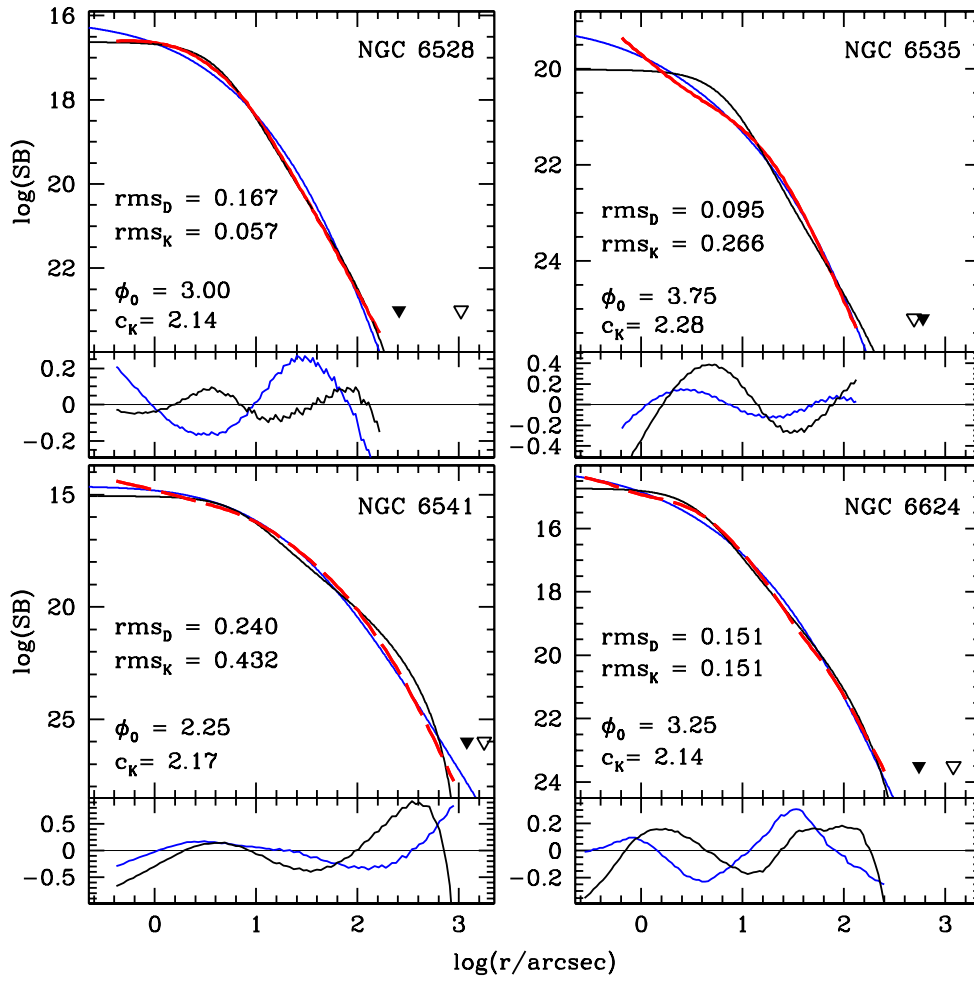


Figure 10. Similar to Figure 4.

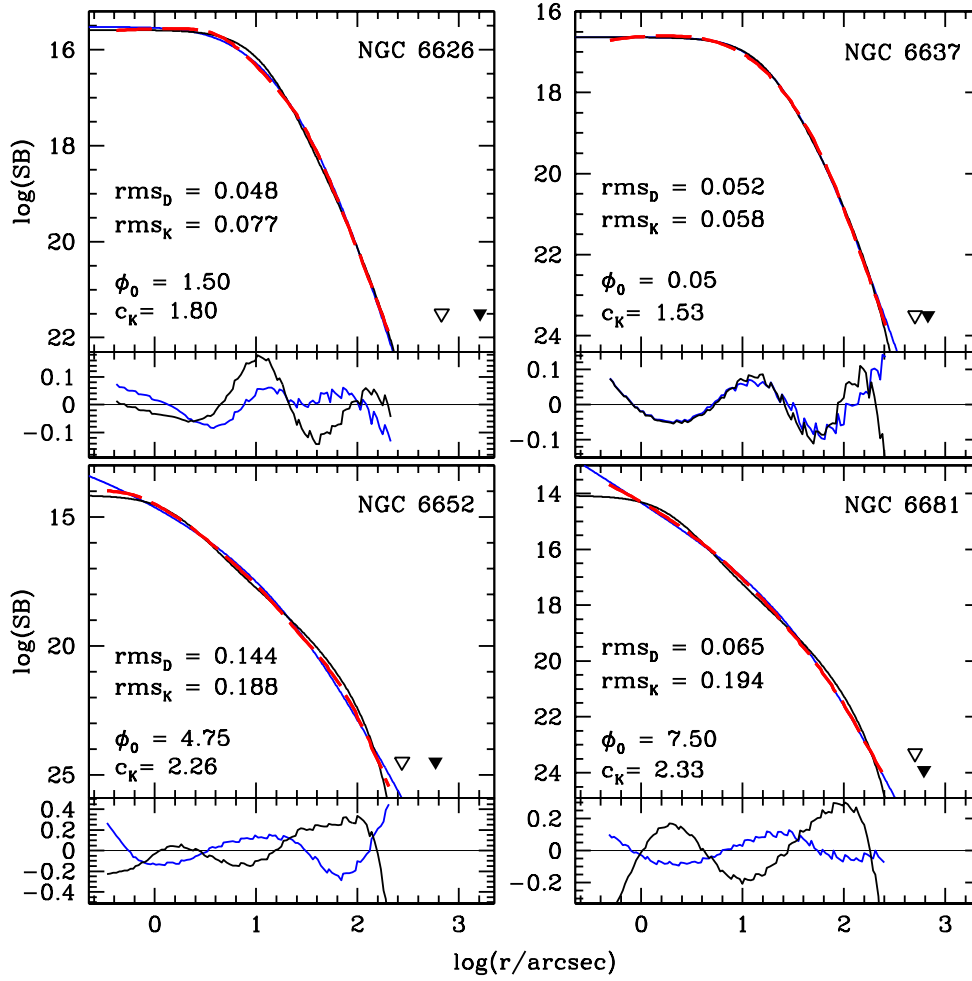


Figure 11. Similar to Figure 4.

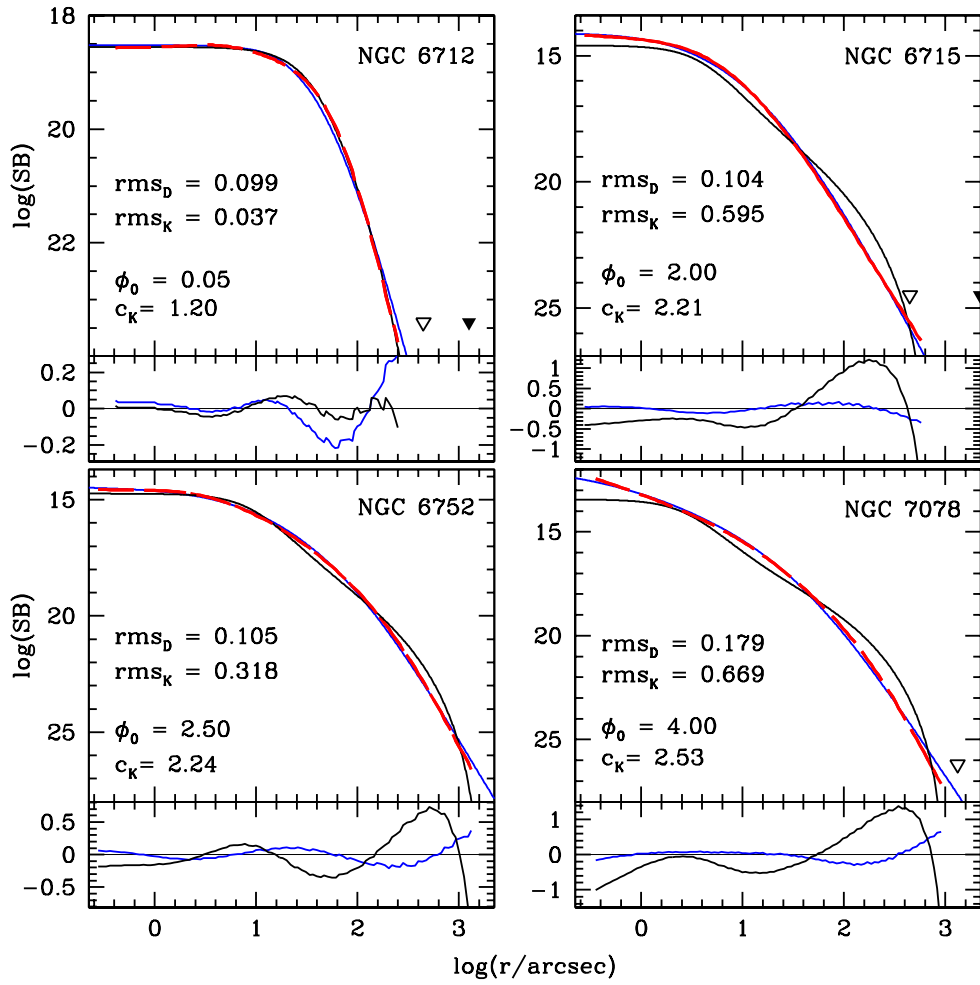


Figure 12. Similar to Figure 4.

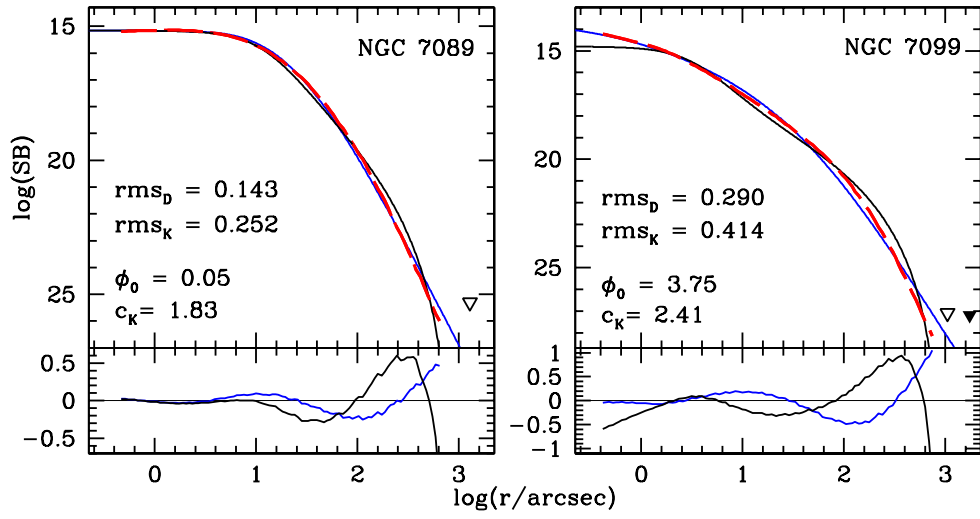
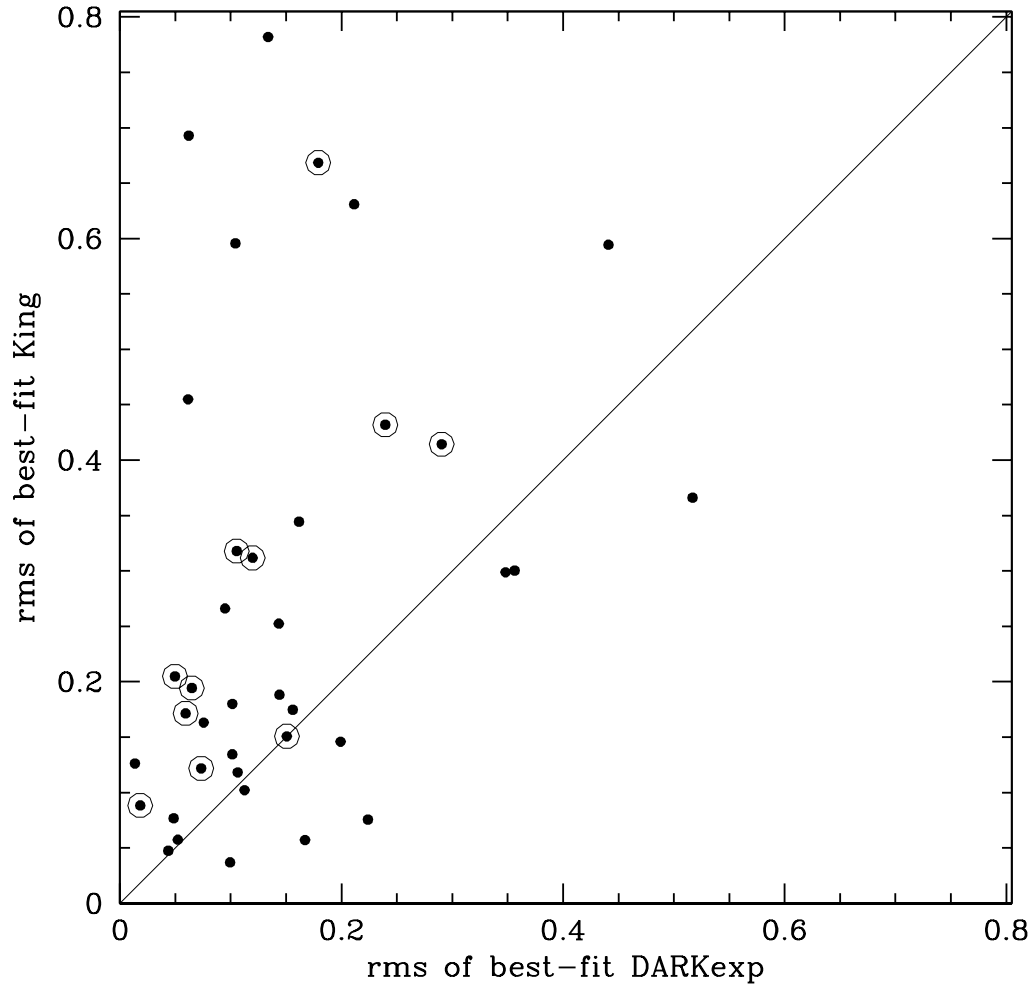
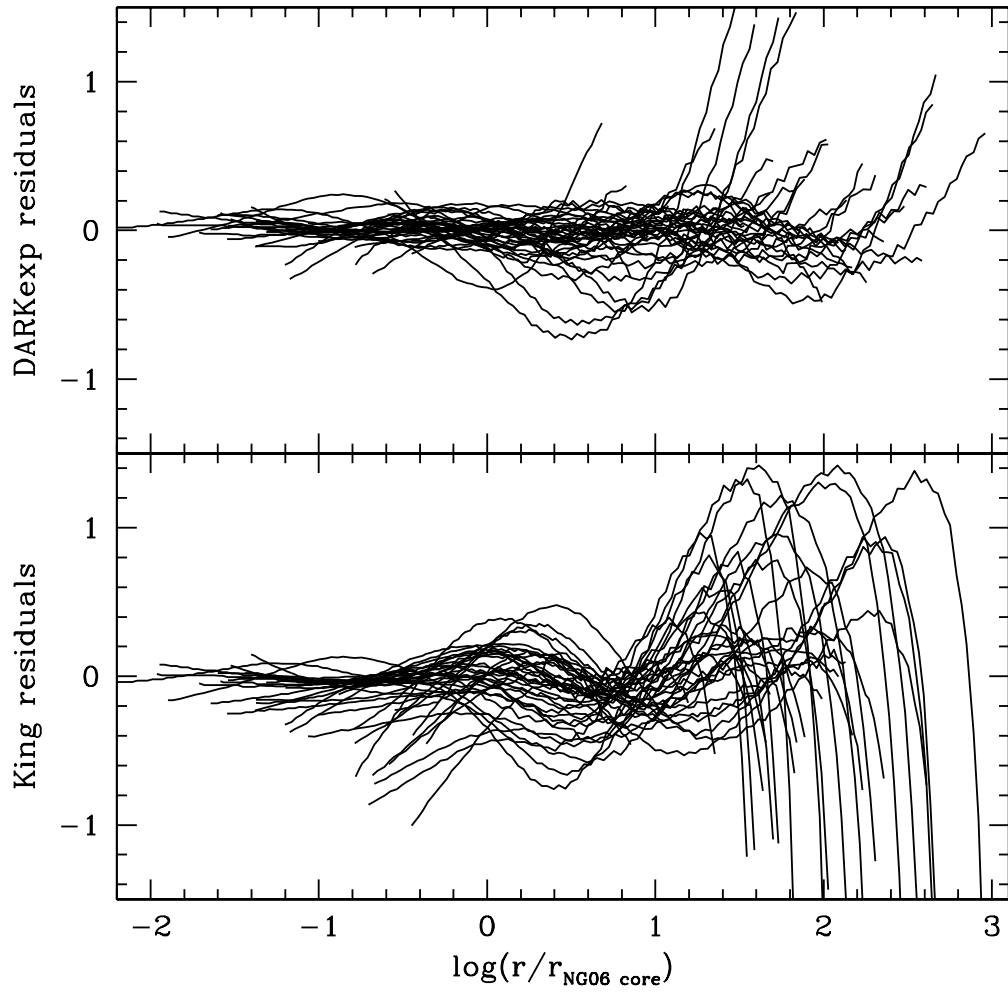


Figure 13. Similar to Figure 4.



**Figure 14.** *Rms* of best-fit King and DARKexp models for 38 GCs. Circled dots represent eleven GCs that are considered to be core-collapsed. Overall, DARKexp models fit GCs considerably better than King models; out of 38 GCs only eight are better fit by King compared to DARKexp.



**Figure 15.** Residuals from best-fit DARkexp and King models for 38 GCs. Radius is normalized by the core radius defined by NG06 as the radius where the SB drops to half its central value. This radius is unrelated to King core radius. In addition to being larger, King residuals also show a more systematic pattern compared to DARkexp residuals.

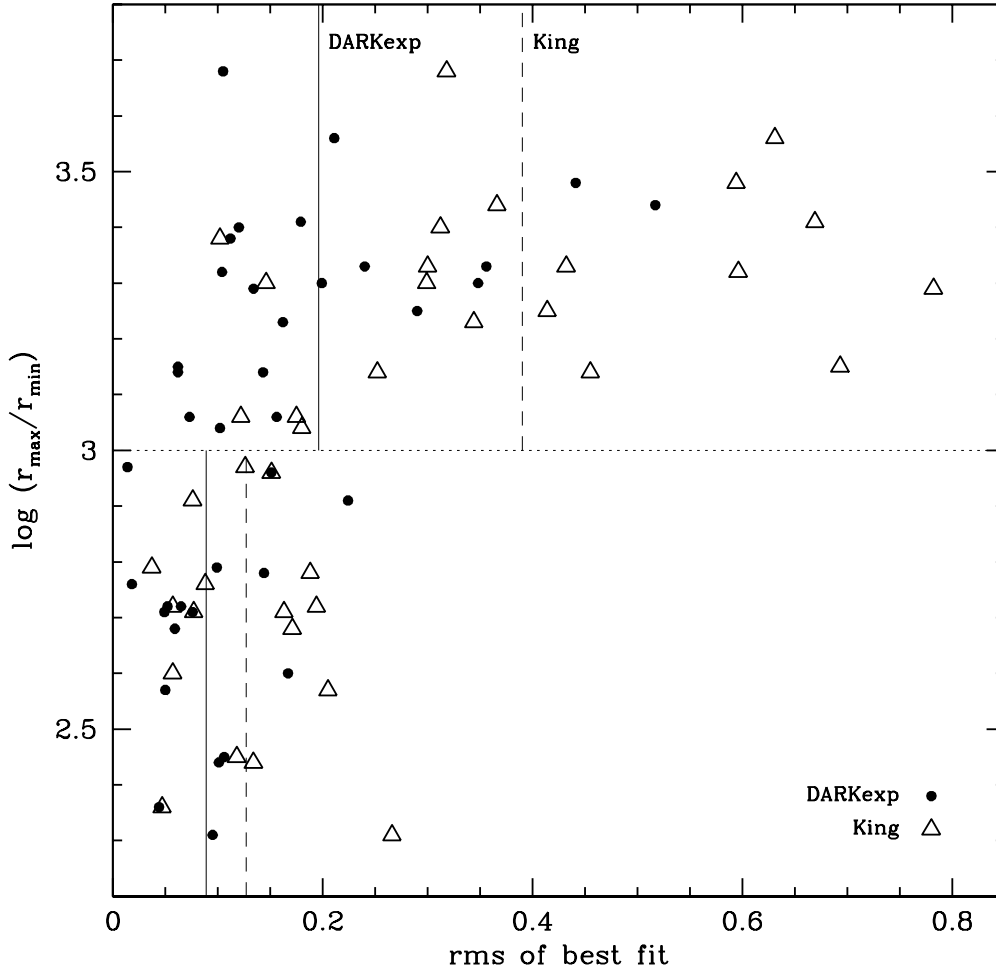


**Figure 16.** Radial range,  $\log(r_{\max}/r_{\min})$  of NG06 data vs.  $rms$  of the best-fit for 38 GCs. DARKexp fits are filled dots, King fits are empty triangles. The horizontal line divides the sample in to two roughly equal sets. In each set the solid vertical line gives the average  $rms$  for the DARKexp fits, while the dashed line give  $rms$  for King fits.



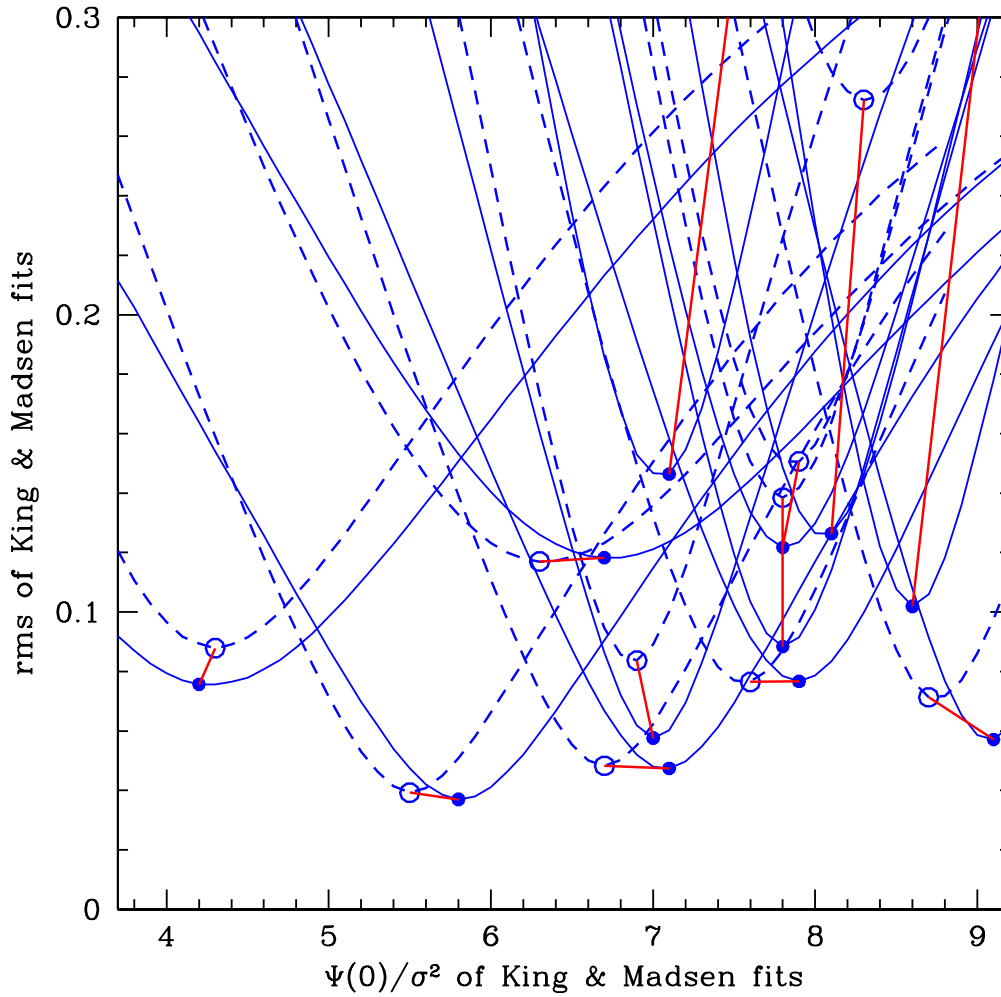


**Figure 17.** Similar to Figure 3, but only for 12 GCs where King models are a good fit. The solid lines and dots represent fits with King models, while the dashed curves and empty circles are the Madsen model fits. Red line segments connect best-fit King and best-fit Madsen models for the same cluster.

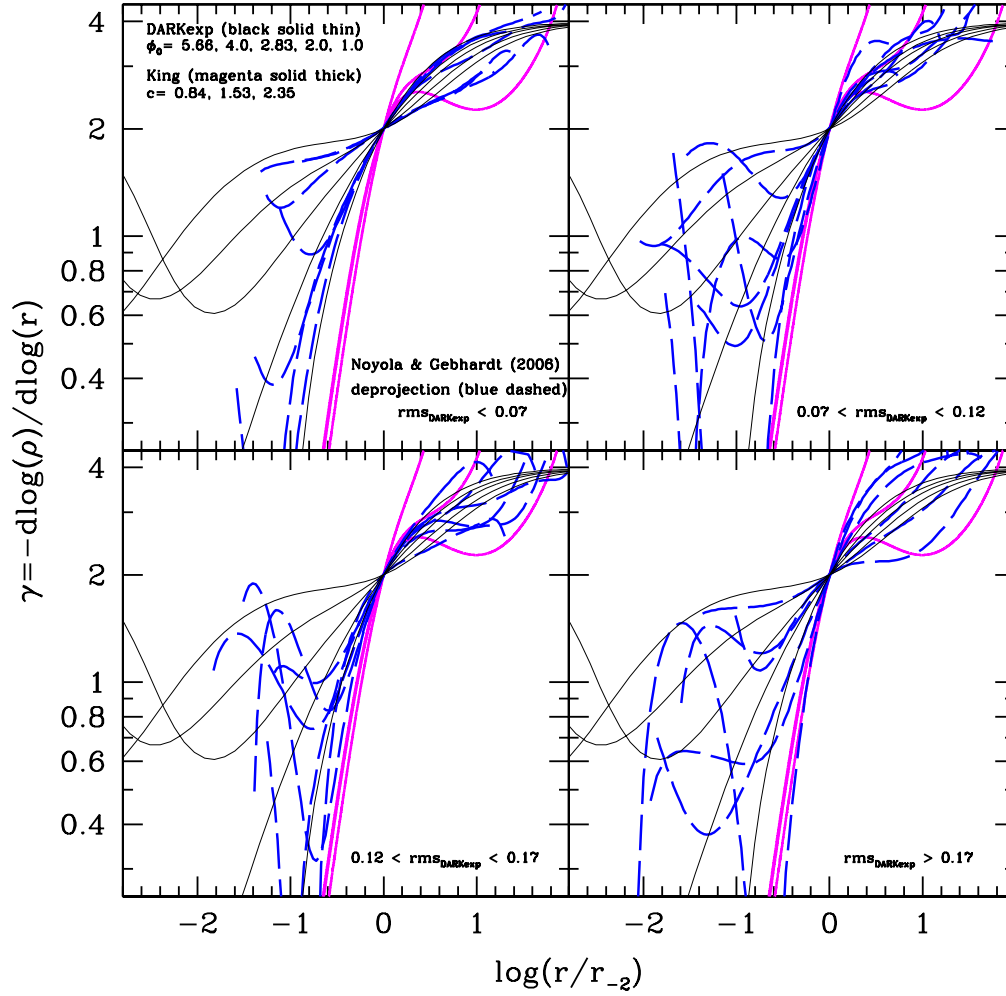


**Figure 18.** 3D log-log density profile slopes for 26 GCs deprojected by Noyola & Gebhardt (2006) (blue dashed) compared to DARKexp (black) and King (magenta) models. All the curves are normalized to have slope  $\gamma = 2$  at  $r = r_{-2}$ . The GCs are grouped into four panels based on how well they are fit by DARKexp;  $rms$  ranges are shown in each panel.

Table 1. DARKexp &amp; King model best-fit parameters for 38 GCs

NGC		$\phi_0$	$c_{D13}$	$rms_D$ (mag/sq.arcsec)	$\frac{\Psi(0)}{\sigma^2}$	$c_K$	$c_{K13}$	$rms_K$ (mag/sq.arcsec)	
104	47 Tuc	1.75	1.16	0.112 (0.050, 0.101)	8.6	2.01	1.47	0.102 (0.011, 0.102)	
1851		2.25	1.35	0.062 (0.030, 0.054)	9.6	2.26	1.78	0.693 (0.331, 0.609)	
1904	M 79	c?	1.50	1.08	0.018 (0.005, 0.018)	7.8	1.77	1.16	0.088 (0.059, 0.065)
2298			0.30	0.80	0.044 (0.041, 0.015)	7.1	1.56	0.86	0.047 (0.042, 0.022)
2808			0.05	0.75	0.441 (0.084, 0.433)	8.3	1.92	1.36	0.594 (0.110, 0.584)
5272	M 3		0.05	0.75	0.211 (0.052, 0.205)	8.8	2.06	1.54	0.631 (0.161, 0.610)
5286			1.00	0.94	0.156 (0.111, 0.109)	7.6	1.71	1.07	0.175 (0.134, 0.112)
5694			1.75	1.16	0.076 (0.043, 0.062)	8.4	1.95	1.40	0.163 (0.053, 0.154)
5824			3.00	1.75	0.134 (0.063, 0.118)	10.1	2.37	1.89	0.782 (0.414, 0.663)
5897			0.05	0.75	0.224 (0.066, 0.214)	4.2	0.87	0.45	0.076 (0.039, 0.065)
5904	M 5		0.05	0.75	0.356 (0.041, 0.354)	8.0	1.83	1.24	0.300 (0.045, 0.297)
6093	M 80		0.75	0.89	0.162 (0.056, 0.152)	8.5	1.98	1.44	0.344 (0.096, 0.331)
6205	M 13		0.05	0.75	0.517 (0.105, 0.506)	7.3	1.62	0.94	0.366 (0.066, 0.360)
6254	M 10		0.05	0.75	0.199 (0.040, 0.195)	7.1	1.56	0.86	0.146 (0.028, 0.143)
6266	M 62	c?	1.75	1.16	0.073 (0.036, 0.064)	7.8	1.77	1.16	0.122 (0.096, 0.075)
6284		c	4.75	2.75	0.059 (0.042, 0.042)	9.8	2.30	1.82	0.171 (0.143, 0.095)
6287			0.50	0.83	0.106 (0.080, 0.070)	6.7	1.44	0.74	0.118 (0.092, 0.074)
6293		c	5.50	3.06	0.050 (0.030, 0.040)	10.5	2.45	1.98	0.205 (0.169, 0.116)
6333	M 9		0.05	0.75	0.102 (0.027, 0.098)	7.3	1.62	0.94	0.180 (0.010, 0.180)
6341	M 92		0.05	0.75	0.348 (0.051, 0.344)	8.1	1.86	1.28	0.299 (0.039, 0.296)
6352			2.50	1.46	0.101 (0.049, 0.089)	11.2	2.59	2.11	0.134 (0.031, 0.131)
6388			1.25	1.01	0.062 (0.030, 0.054)	9.0	2.12	1.61	0.455 (0.154, 0.428)
6397		c	3.50	2.09	0.120 (0.065, 0.100)	9.7	2.28	1.80	0.312 (0.224, 0.217)
6441			1.25	1.01	0.014 (0.006, 0.012)	8.1	1.86	1.28	0.126 (0.036, 0.121)
6528			3.00	1.75	0.167 (0.088, 0.142)	9.1	2.14	1.64	0.057 (0.035, 0.045)
6535			3.75	2.25	0.095 (0.075, 0.059)	9.7	2.28	1.80	0.266 (0.236, 0.123)
6541		c?	2.25	1.35	0.240 (0.094, 0.221)	9.2	2.17	1.67	0.432 (0.192, 0.387)
6624		c	3.25	1.92	0.151 (0.088, 0.123)	9.1	2.14	1.64	0.151 (0.106, 0.107)
6626	M 28		1.50	1.08	0.049 (0.034, 0.035)	7.9	1.80	1.20	0.077 (0.042, 0.064)
6637	M 69		0.05	0.75	0.052 (0.028, 0.044)	7.0	1.53	0.82	0.057 (0.029, 0.049)
6652			4.75	2.75	0.144 (0.076, 0.122)	9.6	2.26	1.78	0.188 (0.089, 0.166)
6681	M 70	c	7.50	3.90	0.065 (0.042, 0.049)	9.9	2.33	1.85	0.194 (0.121, 0.152)
6712			0.05	0.75	0.099 (0.019, 0.098)	5.8	1.20	0.59	0.037 (0.017, 0.033)
6715	M 54		2.00	1.25	0.104 (0.046, 0.094)	9.4	2.21	1.72	0.596 (0.218, 0.554)
6752		c	2.50	1.46	0.105 (0.039, 0.098)	9.5	2.24	1.75	0.318 (0.087, 0.306)
7078	M 15	c	4.00	2.39	0.179 (0.048, 0.173)	10.9	2.53	2.06	0.669 (0.320, 0.587)
7089	M 2		0.05	0.75	0.143 (0.036, 0.139)	8.0	1.83	1.24	0.252 (0.031, 0.250)
7099	M 30	c	3.75	2.25	0.290 (0.078, 0.280)	10.3	2.41	1.94	0.414 (0.170, 0.378)